Letter

Hallmarks of orbital-flavored Majorana states in Josephson junctions based on oxide nanochannels

Alfonso Maiellaro [1,*] Jacopo Settino [2,3,*,†] Claudio Guarcello [1,4,‡] Francesco Romeo [1,4,§] and Roberta Citro [1,4,5,∥]
[1] *Dipartimento di Fisica "E.R. Caianiello," Università di Salerno, Via Giovanni Paolo II, 132, I-84084 Fisciano (SA), Italy*
[2] *Dipartimento di Fisica, Università della Calabria, Via P. Bucci, Arcavacata di Rende (CS), Italy*
[3] *INFN, Gruppo Collegato di Cosenza, Cosenza, Italy*
[4] *INFN, Sezione di Napoli, Gruppo Collegato di Salerno, Salerno, Italy*
[5] *CNR-SPIN, Via Giovanni Paolo II, 132, Fisciano (Sa), Italy*

(Received 2 December 2022; revised 11 March 2023; accepted 31 March 2023; published 17 May 2023)

We investigate the topological properties of a Josephson junction obtained by constraining a two-dimensional electron gas at the oxide interface to form a quasi-one-dimensional conductor. We reveal an anomalous critical current behavior with a magnetic field applied perpendicular to the Rashba spin-orbit one. We relate the observed critical current enhancement at small magnetic fields with the appearance of orbital-flavored Majorana bound states (OMBSs) pinned at the edges of the superconducting leads. Signatures of OMBSs also include a sawtooth profile in the current-phase relation. Our findings allow us to recognize fingerprints of topological superconductivity in noncentrosymmetric materials and confined systems with a spin-orbit interaction. They also explain recent experimental observations for which a microscopic description is still lacking.

DOI: 10.1103/PhysRevB.107.L201405

Introduction. Topological superconductivity (TSC) is an exotic phase of matter in which the fully gapped superconducting bulk hosts Majorana surface states protected by non-Abelian statistics and/or symmetries. In condensed matter systems, the realization of TSC requires the simultaneous presence of an *s*-wave superconducting order (SC) accompanied by the breaking of inversion and time-reversal symmetry. Inversion symmetry breaking might occur in noncentrosymmetric materials and/or confined systems exhibiting large Rashba spin-orbit coupling (SOC). Time-reversal symmetry breaking can be induced by a magnetic order of intrinsic origin or triggered by external magnetic fields. So far, research on TSC has been mainly focused on platforms realized by semiconducting nanowires proximitized by a conventional superconductor [1–10], although other materials and platforms have been recently proposed [11–16].

Several theoretical proposals suggested that the two-dimensional electron gases (2DEGs) formed at the interface between transition metal oxides, such as $LaAlO_3$ and $SrTiO_3$ (LAO/STO) [17–19], are promising candidates for the realization of topological quantum gates, both in 2D [20] and in quasi-one-dimensional (1D) models [21,22]. These ideas are based on the extraordinary properties of these materials and, in particular, the simultaneous presence of strong SOC [23] and 2D SC [24], both electrically tunable [25]. All these phenomena are related to interfacial orbital degrees of freedom, which dominate the oxide 2DEGs physics [26].

The evidence of TSC in oxide 2DEGs has remained elusive up to now. Suggestions in this direction come from the anomalous dependence of the Josephson current on the magnetic field in nanobridges at LAO/STO interfaces [27,28]. One of the most intriguing results is an anomalous enhancement of the critical current pattern, $I_c(H)$, as a function of a magnetic field H orthogonal to the 2DEG plane. An asymmetry with respect to the direction of the applied magnetic field, $I_c(H) \neq I_c(-H)$, is also reported. The anomalous pattern was interpreted as a possible signature of an unconventional component of the order parameter, giving rise to three-channel current with intrinsic phase shifts [28]. On the other hand, a symmetric critical current pattern with a strong enhancement at small magnetic fields has also been observed in a Josephson junction formed by an InAs nanowire proximitized by Ti/Al superconducting leads [7]. In the latter case, it was argued that the observed critical supercurrent increase is compatible with a magnetic field-induced topological transition. Evidence of critical current enhancements as a function of magnetic fields has also been reported for Josephson junctions with ferromagnetic barriers [29,30] and based on gold nanowires [31]. Despite the relevance of these experimental findings, a multiband microscopic model demonstrating the possible connection between the anomalous features of the Josephson current and the topological phase transition is still missing.

Here, we study the transport properties of an oxide-based Josephson junction, made by constraining the 2DEG at the LAO/STO (001) interface [32], to form a quasi-1D system. Our main result is that the strong enhancement of the critical current with applied magnetic field can be associated with the appearance of Majorana bound states with an orbital-flavored internal structure [33], lacking a counterpart in a single-band model. To argue our conclusions, we match the transport properties of the junction with a microscopic spectral analysis of the system. We find that the maximum of the critical current

[*] These authors contributed equally to this work.
Corresponding author: amaiellaro@unisa.it
[†] jacopo.settino@unical.it
[‡] cguarcello@unisa.it
[§] fromeo@unisa.it
[∥] rocitro@unisa.it

pattern at finite magnetic field corresponds to a gap closing in the energy spectrum with the appearance of orbital-flavored Majorana bound states (OMBSs), as signaled by the Majorana polarization analysis. At the same time, the current-phase relations (CPRs) cross over a sawtooth profile. In the presence of OMBSs, we observe nonsinusoidal CPRs and an increasing of the critical current with increasing magnetic fields. Our findings demonstrate that the experimental evidence of the anomalous Josephson pattern discussed in Refs. [28,34] is a strong hallmark of topology.

Theoretical model. We consider a short superconductor-normal-superconductor (SNS) junction realized by constraining the 2DEG at the LAO/STO (001) interface, to form a quasi-1D system. The latter condition is experimentally realizable via appropriate gating of the system. In the absence of superconductivity, the system is described by the nanochannel Hamiltonian $H = H^0 + H^{\rm SO} + H^Z + H^M$ with

$$H^0 = \sum_j \Psi_j^\dagger \big(h^0_{\rm on} \otimes \sigma_0\big)\Psi_j + \Psi_j^\dagger \big(h^0_{\rm hop} \otimes \sigma_0\big)\Psi_{j+1} + {\rm H.c.}, \tag{1}$$

$$H^{\rm SO} = \Delta_{S0} \sum_j \Psi_j^\dagger (l_x \otimes \sigma_x + l_y \otimes \sigma_y + l_z \otimes \sigma_z)\Psi_j, \tag{2}$$

$$H^Z = -i\frac{\gamma}{2} \sum_j \Psi_j^\dagger (l_y \otimes \sigma_0)\Psi_{j+1} + {\rm H.c.}, \tag{3}$$

$$H^M = M_x \sum_j \Psi_j^\dagger (l_x \otimes \sigma_0 + l_0 \otimes \sigma_x)\Psi_j, \tag{4}$$

where we use the t_{2g} orbitals (d_{xy}, d_{yz}, and d_{zx}), while $\Psi_j = (c_{yz,\uparrow,j}, c_{yz,\downarrow,j}, c_{zx,\uparrow,j}, c_{zx,\downarrow,j}, c_{xy,\uparrow,j}, c_{xy,\downarrow,j})^T$ is a vector whose components are the electron annihilation operators for a given spin, orbital, and position. The Hamiltonian terms H^0, $H^{\rm SO}$, H^Z, and H^M represent the kinetic energy, the spin orbit, the inversion-symmetry breaking, and the Zeeman interaction [22]. We consider a nanochannel oriented along the x direction, for which the topological phase is stabilized by a magnetic field perpendicular to the orientation of the orbital Rashba-like field [22,33]. σ_i are the Pauli matrices, while σ_0 indicates the identity matrix. l_x, l_y, and l_z are the projections of the $L = 2$ angular momentum operator onto the t_{2_g} subspace. The analytic expressions of such matrices with those of the hopping Hamiltonians $h^0_{\rm on}$ and $h^0_{\rm hop}$ are reported in the Supplemental Material [35] (see also Refs. [36–39] herein). According to the *ab initio* estimates and on the basis of spectroscopic studies [40–42], in agreement with Ref. [22], we assume $t_1 = 300$, $t_2 = 20$, $\Delta_{\rm SO} = 10$, $\Delta_t = -50$, and $\gamma = 40$ (in units of meV). t_1 and t_2 are the x-directed intraband hopping couplings, respectively, for the yz and zx/xy bands, appearing in H^0. Δ_t denotes the crystal field potential induced by a symmetry lowering from cubic to tetragonal. The latter is also related to inequivalent in-plane and out-of-plane transition metal–oxygen bond lengths, which lowers the on-site energy of the xy band. This set of parameters is also representative of a physical regime with the hierarchy of the electronic energy scales such that $|\Delta_t| > \gamma > \Delta_{\rm SO}$.

In order to introduce superconducting correlations and define the SNS junction geometry, we add to the normal part of the Hamiltonian H the mean-field pairing contribution,

$$H^P = \sum_{j,\alpha} \Delta(j,q)\, c^\dagger_{j,\alpha,\uparrow} c^\dagger_{j,\alpha,\downarrow} + {\rm H.c.}, \tag{5}$$

where α stands for an orbital index and $\Delta(j,q) = \Delta e^{iqj} e^{i\phi_j}$ is a space-dependent gap, taking into account a phase gradient ($\phi_j = \chi_j^L \phi_L + \chi_j^R \phi_R$, with $\chi_j^\alpha = 1$ only when j belongs to the $\alpha = L, R$ electrode) induced by the bias current and a finite momentum effect of the Cooper pair (q). Indeed, for some classes of superconductors, where both inversion and time-reversal symmetries are broken, and in the presence of SOC, it has been shown that Cooper's pairs acquire a finite momentum [43]. Therefore, we have included a spatially modulated superconducting gap, with q continuously determined by the magnetic field ($q = \eta M_x$). The pairing amplitude has been previously determined self-consistently in Ref. [33] as $\Delta = 0.05$, while the phase gradient is given by $\phi = \phi_L - \phi_R$, with $\phi_{L,R}$ the phase of the order parameter of the left and right lead.

The Josephson current of a short SNS junction with translational invariant leads can be efficiently calculated by using the subgap Bogoliubov–de Gennes (BdG) spectrum of a system with truncated superconducting leads as $I(\phi) = -(e/\hbar)\sum_n dE_n/d\phi$ [44], with E_n being the subgap energies of the BdG spectrum. The finite lead approach is valid as long as the short-junction limit is considered [$L_N \ll \xi$, with ξ the Bardeen-Cooper-Schrieffer (BCS) coherence length]. Thus, we set the total size of the system, $L = 2L_S + L_N$, with $L_S \gg \xi$ being the size of the superconducting lead and $L_N \ll L_S$ the normal region size. The maximum (absolute value of minimum) of $I(\phi)$ yields the critical current in the positive (negative) direction. The tight-binding Hamiltonian is numerically treated by using KWANT [45] and solved with the help of NUMPY routines [46]. We explore different electronic regimes defined by the orbital filling and controlled by μ, also varying the Zeeman energy M_x, and the phase difference ϕ. Numerical simulations have been performed by representing the chemical potential in the form $\mu = \mu_0 + e_0$, where e_0, which determines the orbital filling, represents the energy offset measured from the bottom of the band μ_0. An appropriate setting of μ_0 allows us to characterize the orbital-sensitive response of the system.

Numerical results. In the entire Letter we fix $L_S = 1000$, $L_N = 10$ in the unit of the lattice constant. First, we focus on the regime of orbital filling corresponding to the lowest doublet of the energy spectrum with a d_{xy} orbital character [see Fig. 1(a)]. In Figs. 1(b) and 1(c) we report the critical current pattern by varying the Zeeman energy for both $q = 0$ and $q = \eta M_x$, with $\eta \simeq 0.01$ meV^{-1}, deduced by the experimental data in Ref. [28]. Hereafter, we consider an extended Zeeman energy range that is accessible without destroying the superconductivity [47,48] because of an effective Landé g factor that is strongly amplified by confinement effects [49,50]. We notice that, when e_0 is varied in the green shaded area in Fig. 1(a), an anomalous supercurrent enhancement occurs with increasing the Zeeman energy M_x. When e_0 falls in the blue region in Fig. 1(a), a lowering of the critical current for increasing M_x is observed, as in the conventional spin-singlet superconductivity case. The anomalous enhancement

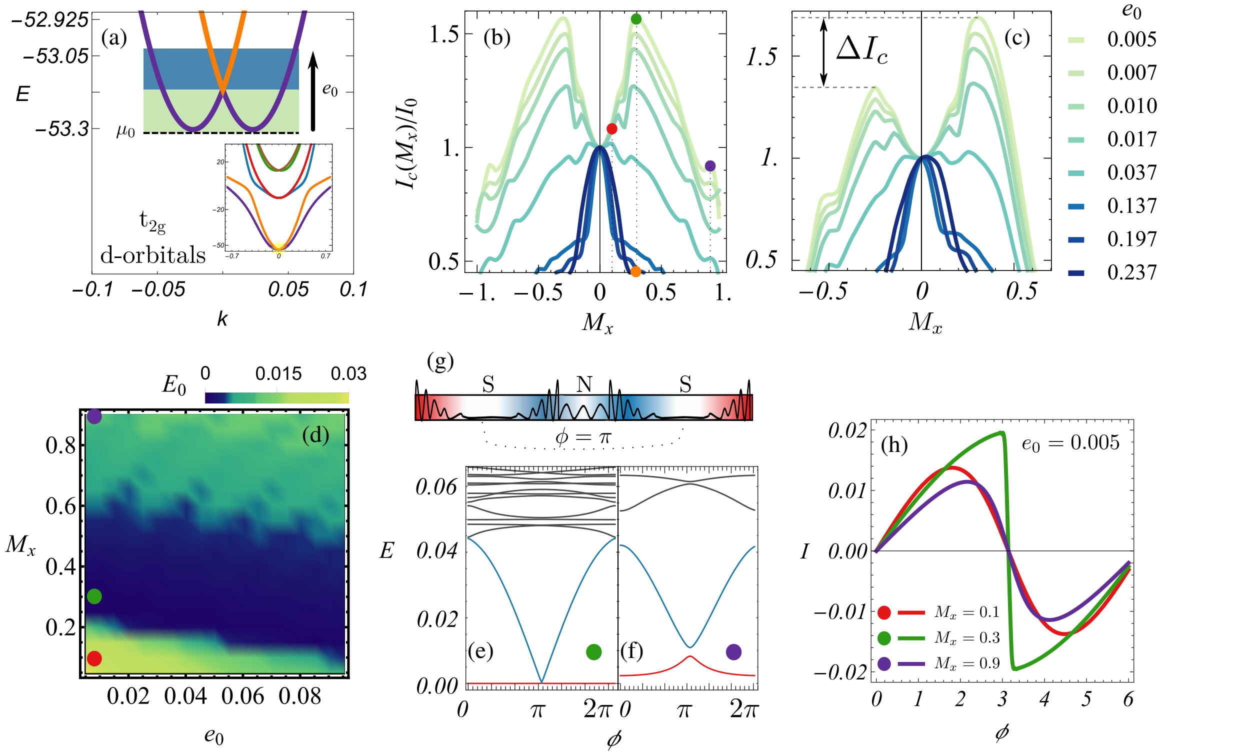

FIG. 1. (a) Sketch of band structure near the Γ point in the Brillouin zone for $M_x = 0$. The six t_{2g} d orbitals, i.e., d_{xy}-like (purple and orange), d_{zx}-like (red and blue), and d_{yz}-like (green and brown), are reported in the inset. The two-tone shaded area (green and blue) shows the lowest doublet. (b) Critical current in the SNS junction as a function of M_x for different filling factors e_0 and $q = 0$. A strong enhancement of I_c occurs at $|M_x| \simeq 0.3$ and low fillings ($e_0 < 0.137$). For $e_0 \geqslant 0.137$, the critical current rapidly decreases with increasing of M_x. (c) Critical current in the SNS junction as in the previous panel and $q = \eta M_x$, with $\eta \sim 0.01$. An asymmetry at changing the field direction is observed. (d) Phase diagram of the junction realized by plotting the lowest-energy level of the half positive sector of the BdG spectrum for $\phi = \pi$, by varying M_x and e_0. Zero-energy region (blue region) corresponds to the emergence of OMBS within each superconductor, and the range of e_0 values corresponds to the green shaded area of (a) (low filling). (e), (f) Low-energy spectrum as a function of the superconducting phase difference ϕ for $M_x = 0.3$ and 0.9, respectively, as indicated by the corresponding green and purple dots. It shows the presence of zero modes in the topological phase (e), while the absence of OMBSs in (f) is clearly traced back to (d). (g) Sketch of the OMBS wave functions in the topological region for $\phi = \pi$, where the blue and red areas indicate the Majorana polarization. (h) CPRs evaluated at the points indicated in (d). CPRs alternate between sinelike behaviors (for $M_x = 0.1, 0.9$) and sawtooth profiles for $M_x = 0.3$, in agreement with topological/trivial phases of the phase diagram [the line's colors correspond to the points of (b) and (d)]. CPRs fulfill the symmetry $I_{M_x}(\phi) = -I_{-M_x}(-\phi)$ (see Supplemental Material [35]).

of the critical current can be understood in terms of a spin-momentum-locking phenomenon. This is realized when the chemical potential lies at the bottom of a Rashba-like band, e.g., see the purple lines in the cartoon in Fig. 1(a). For fillings towards the second band of the orbital doublet, the spin canting increases and consequently imperfect spin-momentum locking is observed. In fact, the bands start to deviate from the ones of the Rashba-like model and the multiband character of the band structure dominates. In this case, the critical current decreases with the magnetic field. Further increasing e_0, when the Fermi energy level cuts the two spin subbands, the spin and momentum degrees of freedom are completely decoupled [see the purple and orange lines in Fig. 1(a)].

Spin-momentum locking is one of the most important properties associated with nontrivial topological states [51,52], and a topological phase transition is expected when e_0 lies at the bottom of the SOC band and M_x increases above a critical magnetic field. The latter is signaled by a gap closing and reopening with the formation of OMBSs at zero energy. The density plot in Fig. 1(d) captures this phenomenology by showing the behavior of the lowest-energy eigenvalue E_0 of the Hamiltonian as a function of e_0 and M_x. The Andreev spectrum as a function of the superconducting phase is shown in Figs. 1(e) and 1(f) for two points of Fig. 1(b). We see a gap closing in Fig. 1(e) indicating a topological phase transition. Indeed, in this regime, the lowest level (red line) is almost insensitive to ϕ and comes from the outer OMBSs of the two superconducting leads. The second energy level (blue line) originates from the inner Majoranas, sketched in Fig. 1(g). It is strongly dispersive with ϕ and becomes degenerate with the lowest-energy level only at $\phi = \pi$. Outside the topological region, both the first and the second energy levels are lifted from zero [see Fig. 1(f)]. For $\phi \neq \pi$, the inner OMBSs hybridize into a fermionic state of finite energy, as discussed below. Figure 1(h) displays the CPRs in the cases highlighted in Fig. 1(d). They show sawtooth profiles for M_x values for which $E_0 = 0$, while for M_x values for which $E_0 \neq 0$, they acquire a sinelike behavior as a function of ϕ [53]. Introducing an effective junction transparency T depending on the value of E_0, we observe that skewed CPRs correspond to $T \to 1$

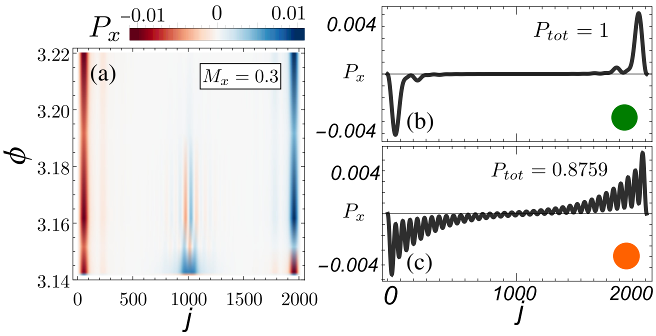

FIG. 2. (a) P_x at $\phi = \pi$ shows the presence of four OMBS at the corners of the two superconductors. For $\phi \gtrsim \pi$ the inner Majoranas disappear, and the Majorana polarization concentrates at the corners (see Supplemental Material [35]). (b), (c) Majorana polarization P_x for $\phi = \pi/40$ and for $M_x = 0.3$ of the lightest green and darkest blue curve of Fig. 1(b), as indicated by the corresponding points. The value of $P_{\rm tot}$ quantifies the topological charge of the exhibited modes.

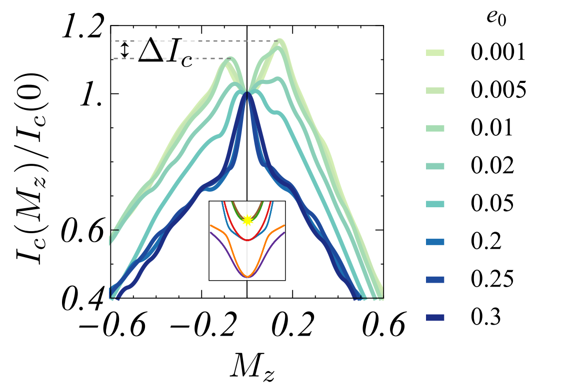

FIG. 3. Critical current in the SNS junction as a function of M_z for different filling factors e_0 starting from the bottom of the highest doublet in the spectrum (see inset) and $q = \eta M_z$, with $\eta = 0.005$. The asymmetric peaks collapse in a single maximum at higher fillings.

and resonant transmission with OMBSs, while $E_0 > 0$ gives sinelike CPRs and $T < 1$ (see Supplemental Material [35]).

The superconducting topological phase can be well characterized by the Majorana polarization (M_p), which measures the quasiparticle weight in the Nambu space. According to Refs. [33,54–56]. $P(j,\omega) = \sum_n (\sum_{\alpha,\sigma} u_{n,j,\alpha,\sigma} v_{n,j,\alpha,\sigma})[\delta(\omega - E_n) + \delta(\omega + E_n)]$, where u and v are the particle and hole components of the Bogoliubov wave function, while α and σ are the orbital and spin indices. Let us note that $P(j,\omega)$ has a nontrivial internal dependence on orbital degrees of freedom, depending on the energy filling e_0. In particular, by choosing $\omega = 0$, the total Majorana polarization $P_{\rm tot} = |\sum_{j=1}^{L/4} P(j,0)|$ is equal to 1 for genuine Majorana fermions. P defines a vector with $P_x(j) = \mathrm{Re}[P(j,0)]$ and $P_y(j) = \mathrm{Im}[P(j,0)]$, and both P_x and P_y are peaked functions at the system edges, i.e., they show OMBSs with opposite topological charge. In particular, Fig. 2(a) shows the appearance of four OMBSs for $\phi = \pi$ [sketched in Fig. 1(g)], while for $\phi \sim \pi + \varepsilon$ (i.e., we set $\varepsilon = 0.05$), the inner OMBSs are fully hybridized and Majorana polarization disappears at the middle of the junction (see Supplemental Material [35]). When $\phi = \pi/40$, fully polarized OMBSs nucleate at the system edges [Fig. 2(b)], while hybridized modes show a polarization loss [Fig. 2(c)]. The scenario described above suggests that the symmetric enhancement of the critical current versus magnetic field curves, reported in Ref. [34], is a fingerprint of a topological phase transition.

The same type of analysis based on the Majorana polarization holds also in the case shown in Fig. 1(c), where an asymmetric enhancement of I_c versus magnetic field is observed. This behavior closely follows the experimental findings of the oxide-based Josephson junction [28,57,58].

Phenomenologically, the asymmetry was ascribed to the inversion symmetry breaking and to the presence of three current channels in the junction, with phases 0, π, and ϕ_0 [28]. The analysis of the CPRs for the two asymmetric maxima still shows a sawtooth profile when the magnetic field approaches the topological phase transition. Interestingly, the critical current pattern is antisymmetric with respect to the inversion of both the magnetic field and the bias current [35]. Thus, the formation of a ϕ junction, and its relevant role for the system response suggested in Ref. [28], is here confirmed.

Finally, in order to explore a different filling regime, we have studied the critical current patterns (see Fig. 3) for chemical potentials corresponding to the upper doublet of bands in the inset of Fig. 1(a). These bands originate from the hybridization of orbitals with d_{zx}, d_{yz} character. As previously shown [33], this band exhibits a transition to the TSC when a magnetic field is applied along the z axis. The critical current pattern shows again a double-maxima structure that coalesce in a single maximum when the energy offset e_0 is moved from the bottom of the doublet to higher values. The asymmetric increase of the current pattern with the applied magnetic field still signals the approach to a topological phase transition with the formation of OMBSs at the edges of the 1D channel (see Supplemental Material [35]).

Conclusion. In summary, we have highlighted that signatures of TSC can be found in the anomalous critical current pattern of short SNS junctions based on oxide nanochannels and, in general, on noncentrosymmetric superconductors. Notably, the topological phase transition is suggested by (i) the enhancement of the critical current by increasing the applied magnetic field perpendicular to the SOC and (ii) the peculiar symmetry by reversing the magnetic field and the bias current (see Supplemental Material [35]). These features are associated with the presence of OMBSs at the edges of the superconducting leads. These topological properties are intertwined to multiband effects, the relevance of which can be adjusted by appropriate gating of the system.

Finally, the microscopic phase transition mechanism, reported in this Letter, appears to be consistent with recent experimental observations of unconventional features of the Josephson current, for which, to date, a microscopic theory is still lacking [7,28].

Acknowledgments. We acknowledge M. Cuoco, A. Geresdi, A. Kalaboukhov, M. Salluzzo, and G. Singh for fruitful discussions.

[1] R. M. Lutchyn, J. D. Sau, and S. Das Sarma, Majorana Fermions and a Topological Phase Transition in Semiconductor-Superconductor Heterostructures, Phys. Rev. Lett. **105**, 077001 (2010).

[2] A. Maiellaro, F. Romeo, C. A. Perroni, V. Cataudella, and R. Citro, Unveiling signatures of topological phases in open Kitaev chains and ladders, Nanomaterials **9**, 894 (2019).

[3] Y. Oreg, G. Refael, and F. von Oppen, Helical Liquids and Majorana Bound States in Quantum Wires, Phys. Rev. Lett. **105**, 177002 (2010).

[4] J. D. Sau, R. M. Lutchyn, S. Tewari, and S. Das Sarma, Generic New Platform for Topological Quantum Computation Using Semiconductor Heterostructures, Phys. Rev. Lett. **104**, 040502 (2010).

[5] R. Aguado, Majorana quasiparticles in condensed matter, Riv. Nuovo Cimento **40**, 523 (2017).

[6] V. Mourik, K. Zuo, S. M. Frolov, S. R. Plissard, E. P. A. M. Bakkers, and L. P. Kouwenhoven, Signatures of Majorana fermions in hybrid superconductor-semiconductor nanowire devices, Science **336**, 1003 (2012).

[7] A. Das, Y. Ronen, Y. Most, Y. Oreg, M. Heiblum, and H. Shtrikman, Zero-bias peaks and splitting in an Al–InAs nanowire topological superconductor as a signature of Majorana fermions, Nat. Phys. **8**, 887 (2012).

[8] M. T. Deng, C. L. Yu, G. Y. Huang, M. Larsson, P. Caroff, and H. Q. Xu, Parity independence of the zero-bias conductance peak in a nanowire based topological superconductor-quantum dot hybrid device, Sci. Rep. **4**, 7261 (2014).

[9] S. M. Albrecht, A. P. Higginbotham, M. Madsen *et al.*, Exponential protection of zero modes in Majorana islands, Nature (London) **531**, 206 (2016).

[10] H. Zhang, C.-X. Liu, S. Gazibegovic, D. Xu, J. A. Logan, G. Wang, N. van Loo, J. D. S. Bommer, M. W. A. de Moor, D. Car *et al.*, Retraction Note: Quantized Majorana conductance, Nature (London) **591**, E30 (2021).

[11] A. Maiellaro and R. Citro, Topological edge states of a Majorana BBH model, Condens. Matter **6**, 15 (2021).

[12] P. Zhang, K. Yaji, T. Hashimoto, Y. Ota, T. Kondo, K. Okazaki, Z. Wang, J. Wen, G. D. Gu, H. Ding *et al.*, Observation of topological superconductivity on the surface of an iron-based superconductor, Science **360**, 182 (2018).

[13] A. Maiellaro, F. Romeo, and R. Citro, Topological phases of a Kitaev tie, Eur. Phys. J. Spec. Top. **229**, 637 (2020).

[14] L. A. Wray, S.-Y. Xu, Y. Xia, D. Hsieh, A. V. Fedorov, Y. S. Hor, R. J. Cava, A. Bansil, H. Lin, and M. Z. Hasan, A topological insulator surface under strong Coulomb, magnetic and disorder perturbations, Nat. Phys. **7**, 32 (2011).

[15] A. Fornieri, A. M. Whiticar, F. Setiawan, E. Portolés, A. C. Drachmann, A. Keselman, S. Gronin, C. Thomas, T. Wang, R. Kallaher *et al.*, Evidence of topological superconductivity in planar Josephson junctions, Nature (London) **569**, 89 (2019).

[16] A. Maiellaro, F. Illuminati, and R. Citro, Topological phases of an interacting Majorana Benalcazar-Bernevig-Hughes model, Condens. Matter **7**, 26 (2022).

[17] A. Barthelemy, N. Bergeal, M. Bibes, A. Caviglia, R. Citro, M. Cuoco, A. Kalaboukhov, B. Kalisky, C. A. Perroni, J. Santamaria *et al.*, Quasi-two-dimensional electron gas at the oxide interfaces for topological quantum physics, Europhys. Lett. **133**, 17001 (2021).

[18] J. Settino, R. Citro, F. Romeo, V. Cataudella, and C. A. Perroni, Ballistic transport through quantum point contacts of multiorbital oxides, Phys. Rev. B **103**, 235120 (2021).

[19] M. Vivek, M. O. Goerbig, and M. Gabay, Topological states at the (001) surface of $SrTiO_3$, Phys. Rev. B **95**, 165117 (2017).

[20] M. S. Scheurer and J. Schmalian, Topological superconductivity and unconventional pairing in oxide interfaces, Nat. Commun. **6**, 6005 (2015).

[21] M. V. Mazziotti, N. Scopigno, M. Grilli, and S. Caprara, Majorana fermions in one-dimensional structures at $LaAlO_3/SrTiO_3$ oxide interfaces, Condens. Matter **3**, 37 (2018).

[22] C. A. Perroni, V. Cataudella, M. Salluzzo, M. Cuoco, and R. Citro, Evolution of topological superconductivity by orbital-selective confinement in oxide nanowires, Phys. Rev. B **100**, 094526 (2019).

[23] A. D. Caviglia, M. Gabay, S. Gariglio, N. Reyren, C. Cancellieri, and J.-M. Triscone, Tunable Rashba Spin-Orbit Interaction at Oxide Interfaces, Phys. Rev. Lett. **104**, 126803 (2010).

[24] N. Reyren, S. Thiel, A. D. Caviglia, L. F. Kourkoutis, G. Hammerl, C. Richter, C. W. Schneider, T. Kopp, A.-S. Rüetschi, D. Jaccard *et al.*, Superconducting interfaces between insulating oxides, Science **317**, 1196 (2007).

[25] A. Caviglia, S. Gariglio, N. Reyren, D. Jaccard, T. Schneider, M. Gabay, S. Thiel, G. Hammerl, J. Mannhart, and J.-M. Triscone, Electric field control of the $LaAlO_3/SrTiO_3$ interface ground state, Nature (London) **456**, 624 (2008).

[26] M. Salluzzo, J. C. Cezar, N. B. Brookes, V. Bisogni, G. M. De Luca, C. Richter, S. Thiel, J. Mannhart, M. Huijben, A. Brinkman *et al.*, Orbital Reconstruction and the Two-Dimensional Electron Gas at the $LaAlO_3/SrTiO_3$ Interface, Phys. Rev. Lett. **102**, 166804 (2009).

[27] D. Stornaiuolo, D. Massarotti, R. Di Capua, P. Lucignano, G. P. Pepe, M. Salluzzo, and F. Tafuri, Signatures of unconventional superconductivity in the $LaAlO_3/SrTiO_3$ two-dimensional system, Phys. Rev. B **95**, 140502(R) (2017).

[28] G. Singh, C. Guarcello, E. Lesne, D. Winkler, T. Claeson, T. Bauch, F. Lombardi, A. Caviglia, R. Citro, M. Cuoco *et al.*, Gate-tunable pairing channels in superconducting non-centrosymmetric oxides nanowires, npj Quantum Mater. **7**, 2 (2022).

[29] M. Weides, M. Kemmler, H. Kohlstedt, R. Waser, D. Koelle, R. Kleiner, and E. Goldobin, $0-\pi$ Josephson Tunnel Junctions with Ferromagnetic Barrier, Phys. Rev. Lett. **97**, 247001 (2006).

[30] M. Kemmler, M. Weides, M. Weiler, M. Opel, S. T. B. Goennenwein, A. S. Vasenko, A. A. Golubov, H. Kohlstedt, D. Koelle, R. Kleiner, and E. Goldobin, Magnetic interference patterns in $0-\pi$ superconductor/insulator/ferromagnet/superconductor Josephson junctions: Effects of asymmetry between 0 and π regions, Phys. Rev. B **81**, 054522 (2010).

[31] J. Wang, Z. Wang, and P. Wang, Magnetic field enhanced critical current and subharmonic structures in dissipative superconducting gold nanowires, Quantum Front. **1**, 21 (2022).

[32] Y. Fukaya, S. Tamura, K. Yada, Y. Tanaka, P. Gentile, and M. Cuoco, Interorbital topological superconductivity in spin-orbit coupled superconductors with inversion symmetry breaking, Phys. Rev. B **97**, 174522 (2018).

[33] J. Settino, F. Forte, C. A. Perroni, V. Cataudella, M. Cuoco, and R. Citro, Spin-orbital polarization of Majorana edge states in oxide nanowires, Phys. Rev. B **102**, 224508 (2020).

[34] J. Tiira, E. Strambini, M. Amado, S. Roddaro, P. San-Jose, R. Aguado, F. S. Bergeret, D. Ercolani, L. Sorba, and F. Giazotto, Magnetically-driven colossal supercurrent enhancement in InAs nanowire Josephson junctions, Nat. Commun. **8**, 14984 (2017).

[35] See Supplemental Material at http://link.aps.org/supplemental/10.1103/PhysRevB.107.L201405 for technical details and additional results on the connection between critical currents and OMBSs.

[36] F. Nichele, E. Portolés, A. Fornieri, A. M. Whiticar, A. C. C. Drachmann, S. Gronin, T. Wang, G. C. Gardner, C. Thomas, A. T. Hatke, M. J. Manfra, and C. M. Marcus, Relating Andreev Bound States and Supercurrents in Hybrid Josephson Junctions, Phys. Rev. Lett. **124**, 226801 (2020).

[37] S. Kashiwaya, K. Saitoh, H. Kashiwaya, M. Koyanagi, M. Sato, K. Yada, Y. Tanaka, and Y. Maeno, Time-reversal invariant superconductivity of Sr_2RuO_4 revealed by Josephson effects, Phys. Rev. B **100**, 094530 (2019).

[38] A. A. Golubov, M. Y. Kupriyanov, and E. Il'ichev, The current-phase relation in Josephson junctions, Rev. Mod. Phys. **76**, 411 (2004).

[39] A. Barone and G. Paterno, *Physics and Applications of the Josephson Effect* (Wiley, New York, 1982).

[40] Y.-Y. Pai, A. Tylan-Tyler, P. Irvin, and J. Levy, Physics of $SrTiO_3$-based heterostructures and nanostructures: a review, Rep. Prog. Phys. **81**, 036503 (2018).

[41] Z. Zhong, A. Tóth, and K. Held, Theory of spin-orbit coupling at $LaAlO_3/SrTiO_3$ interfaces and $SrTiO_3$ surfaces, Phys. Rev. B **87**, 161102(R) (2013).

[42] A. Joshua, S. Pecker, J. Ruhman, E. Altman, and S. Ilani, A universal critical density underlying the physics of electrons at the $LaAlO_3/SrTiO_3$ interface, Nat. Commun. **3**, 1129 (2012).

[43] N. F. Q. Yuan and L. Fu, Supercurrent diode effect and finite-momentum superconductors, Proc. Natl. Acad. Sci. USA **119**, e2119548119 (2022).

[44] J. Cayao, P. San-Jose, A. M. Black-Schaffer, R. Aguado, and E. Prada, Majorana splitting from critical currents in Josephson junctions, Phys. Rev. B **96**, 205425 (2017).

[45] C. W. Groth, M. Wimmer, A. R. Akhmerov, and X. Waintal, Kwant: a software package for quantum transport, New J. Phys. **16**, 063065 (2014).

[46] T. E. Oliphant, *Guide to NumPy* (Trelgol, 2006), https://www.bibsonomy.org/bibtex/f13bb8f9237574e5678cedd1b36c4175.

[47] S. C. Shen, B. B. Chen, H. X. Xue, G. Cao, C. J. Li, X. X. Wang, Y. P. Hong, G. P. Guo, R. F. Dou, C. M. Xiong *et al.*, Gate dependence of upper critical field in superconducting (110) $LaAlO_3/SrTiO_3$ interface, Sci. Rep. **6**, 28379 (2016).

[48] R. Erlandsen, R. T. Dahm, F. Trier, M. Scuderi, E. Di Gennaro, A. Sambri, C. K. Reffeldt Kirchert, N. Pryds, F. M. Granozio, and T. S. Jespersen, A two-dimensional superconducting electron gas in freestanding $LaAlO_3/SrTiO_3$ micromembranes, Nano Lett. **22**, 4758 (2022).

[49] C.-K. Wang and K.-F. Berggren, Spin splitting of subbands in quasi-one-dimensional electron quantum channels, Phys. Rev. B **54**, R14257 (1996).

[50] A. V. Bjørlig, D. J. Carrad, G. E. D. K. Prawiroatmodjo, M. von Soosten, Y. Gan, Y. Chen, N. Pryds, J. Paaske, and T. S. Jespersen, *g*-factors in $LaAlO_3/SrTiO_3$ quantum dots, Phys. Rev. Mater. **4**, 122001(R) (2020).

[51] J. Tian, I. Childres, H. Cao, T. Shen, I. Miotkowski, and Y. P. Chen, Topological insulator based spin valve devices: Evidence for spin polarized transport of spin-momentum-locked topological surface states, Solid State Commun. **191**, 1 (2014).

[52] J.-R. Chen, P. L. Tse, I. N. Krivorotov, and J. G. Lu, Spin-momentum locking induced non-local voltage in topological insulator nanowire, Nanoscale **12**, 22958 (2020).

[53] P. Marra, R. Citro, and A. Braggio, Signatures of topological phase transitions in Josephson current-phase discontinuities, Phys. Rev. B **93**, 220507(R) (2016).

[54] C. Bena, Testing the formation of Majorana states using Majorana polarization, C. R. Phys. **18**, 349 (2017).

[55] S. Głodzik, N. Sedlmayr, and T. Domański, How to measure the Majorana polarization of a topological planar Josephson junction, Phys. Rev. B **102**, 085411 (2020).

[56] A. Maiellaro, F. Romeo, and R. Citro, Effects of geometric frustration in Kitaev chains, Eur. Phys. J. Plus **136**, 627 (2021).

[57] G. M. De Luca, R. Di Capua, E. Di Gennaro, F. M. Granozio, D. Stornaiuolo, M. Salluzzo, A. Gadaleta, I. Pallecchi, D. Marrè, C. Piamonteze *et al.*, Transport properties of a quasi-two-dimensional electron system formed in $LaAlO_3/EuTiO_3/SrTiO_3$ heterostructures, Phys. Rev. B **89**, 224413 (2014).

[58] Both Refs. [28,34] consider a magnetic field along the z direction. We have verified that changing the magnetic field direction from x to z has no physical significance in the emerging phenomenon and the latter considerations still remain true. However, in view of the nontrivial multiband effects, small quantitative differences are shown for $M_i \geqslant 0.3$ ($i = x, z$). Figure 4 of the Supplemental Material compares the two directions of the magnetic field.